DIGITAL ACCESS TO SCHOLARSHIP AT HARVARD
DASH.HARVARD.EDU

HARVARD LIBRARY
Office for Scholarly Communication

Potentiating antibacterial activity by predictably enhancing endogenous microbial ROS production

Citation
Brynildsen, Mark P., Jonathan A. Winkler, Catherine S. Spina, I. Cody MacDonald, and James J. Collins. 2012. "Potentiating antibacterial activity by predictably enhancing endogenous microbial ROS production." Nature biotechnology 31 (2): 160-165. doi:10.1038/nbt.2458. http://dx.doi.org/10.1038/nbt.2458.

Published Version
doi:10.1038/nbt.2458

Permanent link
http://nrs.harvard.edu/urn-3:HUL.InstRepos:11855791

Terms of Use
This article was downloaded from Harvard University's DASH repository, and is made available under the terms and conditions applicable to Other Posted Material, as set forth at http://nrs.harvard.edu/urn-3:HUL.InstRepos:dash.current.terms-of-use#LAA

Share Your Story

The Harvard community has made this article openly available.
Please share how this access benefits you. Submit a story .

Accessibility

NIH Public Access
Author Manuscript
Nat Biotechnol. Author manuscript; available in PMC 2013 August 01.

Published in final edited form as:
Nat Biotechnol. 2013 February ; 31(2): 160–165. doi:10.1038/nbt.2458.

Potentiating antibacterial activity by predictably enhancing endogenous microbial ROS production

Mark P. Brynildsen[1,2,3], **Jonathan A. Winkler**[1,4,2], **Catherine S. Spina**[1,5,6], **I. Cody MacDonald**[1], and **James J. Collins**[1,4,5,6]

[1]Howard Hughes Medical Institute, Department of Biomedical Engineering, and Center for BioDynamics, Boston University, Boston, MA 02215, USA

[4]Program in Molecular Biology, Cell Biology, and Biochemistry, Boston University, Boston, MA 02215, USA

[5]Boston University School of Medicine, 715 Albany Street, Boston, MA 02118, USA

[6]Wyss Institute for Biologically Inspired Engineering, Harvard University, Boston, MA 02118, USA

Abstract

The ever-increasing incidence of antibiotic-resistant infections combined with a weak pipeline of new antibiotics has created a global public health crisis[1]. Accordingly, novel strategies for enhancing our antibiotic arsenal are needed. As antibiotics kill bacteria in part by inducing reactive oxygen species (ROS)[2–4], we reasoned that targeting microbial ROS production might potentiate antibiotic activity. Here we show that ROS production can be predictably enhanced in *Escherichia coli*, increasing the bacteria's susceptibility to oxidative attack. We developed an ensemble, genome-scale metabolic modeling approach capable of predicting ROS production in *E. coli*. The metabolic network was systematically perturbed and its flux distribution analyzed to identify targets predicted to increase ROS production. *In silico*–predicted targets were experimentally validated and shown to confer increased susceptibility to oxidants. Validated targets also increased susceptibility to killing by antibiotics. This work establishes a systems-based method to tune ROS production in bacteria and demonstrates that increased microbial ROS production can potentiate killing by oxidants and antibiotics.

Reactive oxygen species (ROS) can damage DNA, RNA, proteins and lipids, resulting in cell death when the level of ROS exceeds an organism's detoxification and repair capabilities. Despite this danger, aerobically growing bacteria endogenously generate ROS as a metabolic by-product, a risk balanced by an increased efficiency and yield of energy from growth substrates. At least two possible mechanisms exist to manipulate bacterial ROS metabolism and achieve increased sensitivity to oxidative attack: (1) amplification of endogenous ROS production, and (2) impairment of detoxification and repair systems. Whereas removal of detoxification and repair systems has been shown to increase susceptibility to oxidants[5, 6], antibiotics[7] and immunity[8, 9], manipulation of endogenous

Correspondence should be addressed to James J. Collins (jcollins@bu.edu).
[2]These authors contributed equally to this work
[3]Present address: Department of Chemical and Biological Engineering, Princeton University, Princeton, NJ, 08544

Author Contributions. M.P.B, J.A.W, and J.J.C designed the study, analyzed the results, and wrote the manuscript. Experiments were performed by M.P.B, J.A.W, C.S.S, and I.C.M.

Note: Supplementary information is available at http://www.nature.com/doifinder/10.1038/nbt.xxx.

Competing financial interests: The authors declare competing financial interests in the form of US Patent Application No. 61/583,662.

NIH-PA Author Manuscript
NIH-PA Author Manuscript
NIH-PA Author Manuscript

NIH-PA Author Manuscript

NIH-PA Author Manuscript

NIH-PA Author Manuscript

ROS production remains largely unexplored. Endogenous ROS production has long been appreciated as a factor influencing the ability of an organism to survive oxidative stress[10], but an inability to predict the outcome of genetic and environmental perturbations on ROS production[11] has hampered exploration of this phenomenon as an antimicrobial adjuvant. This inability derives from a limited systems-level understanding of a potentially, expansive and highly integrated biochemical reaction network. In this study, we sought to tune *E. coli* metabolism for increased ROS production (specifically, O_2^- and H_2O_2) and to determine whether this effect can potentiate oxidative stress and antibiotic activity. Our goal was not to overwhelm the oxidative detoxification and repair capabilities of *E. coli* with endogenously generated ROS, but rather to increase endogenous production such that the ability of *E. coli* to cope with exogenous oxidative stress would be compromised. We hypothesized that such a strategy would broadly potentiate antimicrobials that harness oxidative stress and provide a general approach for the discovery of antimicrobial adjuvants. To achieve this goal, we developed an ensemble, genome-scale modeling approach to quantitatively estimate ROS production from *E. coli* metabolism (Fig. 1).

The sources for the majority of endogenous ROS produced by *E. coli* remain elusive[11]. The removal of enzymes that generate ROS *in vitro* has had seemingly little effect on whole-cell ROS production[11]. This can be explained by the potential scope of ROS generators. Previous studies have demonstrated that O_2^- and H_2O_2 can be produced when O_2 abstracts electrons from reduced flavin, quinol and transition metal functional groups[12, 13]. Inspection of *E. coli* metabolism for enzymes that use these electron carriers identified 133 reactions, spanning many metabolic pathways, with the potential to generate ROS in the presence of O_2 (see Supplementary Table 1 online). The number of potential ROS-generating reactions is of comparable size to the number of reactions that generate ATP/ADP, NAD/H, and NADP/H, suggesting that ROS could play a crucial, highly integrated role in bacterial metabolism. To predictably modify the production of such highly connected metabolites, a quantitative systems-level approach is required, as even removal of enzymes that endogenously produce ROS may increase or decrease production depending on the redistribution of metabolic flux on the remaining ROS-generating enzymes[11].

Systems-level metabolic modeling has been used extensively to optimize the production of desirable metabolites, and has significantly impacted the fields of biotechnology, metabolic discovery and microbiology[14]. In this study, we employed flux balance analysis (FBA) with genome-scale metabolic models (GSMM) to simulate systems-level ROS production in *E. coli*. In FBA, reaction stoichiometries are used to define a metabolic solution space, and linear programming identifies a flux distribution within that space that optimizes an objective function, such as biomass generation. Accuracy within the stoichiometric reaction network is critical to the performance of constraint-based techniques[15, 16]. Current metabolic reconstructions include consumption reactions, such as superoxide dismutase and catalase, and generation reactions involved in cofactor biosynthesis and alternate carbon metabolism, but are devoid of generation reactions that account for the majority of ROS produced[17]. To construct a metabolic model capable of estimating ROS production, we added 266 additional ROS production reactions to the *E. coli* GSMM[17] one O_2^- and one H_2O_2 producing reaction for each of the 133 potential sources (see Methods, Supplementary Methods and Supplementary Table 1 online). These potential ROS sources included all enzymes known to generate H_2O_2 and O_2^- in *E. coli* [11, 13, 17, 18], and this framework allowed separate (independent species balances) but simultaneous modeling of H_2O_2 and O_2^- production in *E. coli*.

Optimization of an objective function is a critical feature of constraint-based techniques, and maximizing for biomass generation has proven to be effective in predicting redistribution of metabolic flux[19]. However, when presented with competing pathways, constraint-based

NIH-PA Author Manuscript

NIH-PA Author Manuscript

NIH-PA Author Manuscript

methods will identify the most efficient pathway in terms of cellular resources as the one that carries flux. ROS-generating reactions are less efficient competing pathways where reducing equivalents are lost to O_2 instead of being transferred to the intended acceptor. Therefore, addition of ROS-generating reactions to a GSMM is necessary to model ROS metabolism, but insufficient because the reactions will not carry flux (see Supplementary Methods online). To address this, we recognized that ROS-generating reactions are coupled to their more efficient counterpart, in the sense that initial electron transfer from reactant to electron carrier proceeds normally and is dictated by requirements for the intended products, and that it is the promiscuity of the reduced electron carrier with O_2 that generates ROS. Thus, ROS flux is a function of the number of electrons transferred to the electron carrier, and consequently dependent on the reaction flux of the intended reaction. Therefore, in this study, the flux of O_2^- and H_2O_2 from ROS-generating enzyme$_i$ was assumed to be proportional to the reaction flux, v_i. This assumption results in proportionality between ROS flux from enzyme$_i$ and the number of electrons transferred by enzyme$_i$, and is accomplished by coupling the intended enzyme reaction to both its O_2^- and H_2O_2 side-reactions (see Methods and Supplementary Methods online). This coupling requires specification of the proportion of electrons that flow to O_2 to form O_2^- and H_2O_2 for each of the 133 potential ROS sources. These values vary significantly from enzyme to enzyme[12, 20], and are largely undefined owing to the absence of *in vivo* measurements. With this indeterminacy in mind, we employed an ensemble approach.

Two ensembles of ROS-GSMMs were constructed, each with 1,000 different models (see Supplementary Methods online). The proportions of electron flow from reaction$_i$ to generate O_2^- and H_2O_2 were captured by the constants c_{i,o_2^-} and $c_{i,\,H_2O_2}$ (see Supplementary Methods online). One ensemble derived these constants from a Gaussian distribution in order to model a distributed ROS production network (many significant generators), whereas the other ensemble derived these constants from an exponential distribution to model a centralized ROS production network (few significant generators). Further, it was specified that ROS could only be produced from these reactions and not consumed, with the exception of O_2^- attack of Fe-S centers, and that the *in silico* O_2^- and H_2O_2 production rates of the wildtype GSMM had to match the best available experimental estimates (see Methods and Supplementary Methods online). Thus, every stoichiometric reaction network within the ensembles had the exact same production rate of O_2^- and H_2O_2 for its wildtype GSMM. Also, the existence of alternative optimal solutions for ROS production of each wildtype network was examined using flux varability analysis (FVA). At a biomass production rate of 100%, all wildtype networks generate a unique solution for the flux of H_2O_2 and O_2^- (see Supplementary Methods online).

With these ensembles, we explored *in silico* how perturbations to the metabolic network alter basal ROS production. We performed a systematic gene-deletion analysis in which genes were removed one at a time and reaction fluxes recalculated, while optimizing for biomass (see Methods and Supplementary Methods online). This provided quantitative distributions of ROS production (H_2O_2 and O_2^-) from mutant *E. coli* (Fig. 1) and allowed identification of deletions likely to alter basal ROS production, as measured by the mean ROS production level (Fig. 2a,b andSupplementary Fig. 1a). To account for variable growth rates of mutant strains, we normalized ROS flux by biomass production (BM), and calculations are therefore H_2O_2/BM and O_2^-/BM (mmol/gDW produced). From our analysis of aerobic glucose minimal media, the gene deletions identified as being most likely to increase ROS production encoded for ATP synthase (*atpA-I*), pyruvate dehydrogenase (*aceEF, lpd*), NADH dehydrogenase complex I (*nuoABCE-N*), glutamate dehydrogenase (*gdhA*), cytochrome *bo* (*cyoABCD*), and triose phosphate isomerase (*tpiA*). Investigation of the flux distributions for these mutants identified a general trend for ROS production where predicted increases correlated with inefficiencies in the production or usage of ATP.

NIH-PA Author Manuscript

NIH-PA Author Manuscript

NIH-PA Author Manuscript

To validate our approach and *in silico* analysis, we experimentally tested a series of gene deletions that encode enzymes within glycolysis, the pentose-phosphate pathway, Entner-Doudoroff pathway, TCA cycle, glyoxylate shunt, aerobic respiration, acetate metabolism and glutamate metabolism (Fig. 2c,d and Supplementary Fig. 1b). This collection of enzymes included those predicted to increase ROS (targets) as well as those predicted to leave ROS production unchanged (negative controls). We note that our predictions include all twenty-one genetic mutants tested, both targets and negative controls, and that only those enzymes that were experimentally tested are color-coded in Figure 2 and Supplementary Figure 1. Isozymes selected for testing were based on literature evidence that suggested their removal would most closely reflect model assumptions, and deletions of pyruvate dehydrogenase and triose-phosphate isomerase were not tested owing to an inability to grow in minimal glucose media (see Supplementary Methods online).

To measure O_2^-, we employed a SoxR-controlled GFP-reporter system, whereas to measure H_2O_2, we used both an OxyR-controlled GFP-reporter system and the direct-sensing HyPer protein (Methods). Our experimental results show between 80–90% qualitative agreement with our *in silico* predictions of H_2O_2 and O_2^- production (Fig. 2 and Supplementary Fig. 1; Correct predictions: *dps*-GFP: 19/21, *soxS*-GFP: 17/21, HyPer: 17/21). The probabilities that these levels of agreement would have occurred by chance, using the null hypothesis that random segregation of the 21 genes into targets and negative controls would match experimental results as well as predictions from our modeling approach, are 3.7×10^{-4} (*dps*-GFP), 1.0×10^{-2} (*soxS*-GFP), and $6.2\times^{-3}$ (HyPer) (Methods). These experimental results suggest that our systems-level, ensemble approach enables predictable tuning of ROS production in *E. coli*.

We next sought to determine if increased basal production of O_2^- and/or H_2O_2 can translate into increased killing by oxidants. The oxidants we tested were O_2^-(generated via menadione), H_2O_2, and NaOCl (bleach). O_2^- and H_2O_2 were chosen owing to their inclusion in the model and importance for antibiotic action[3], and NaOCl was chosen owing to its use as a biocide. Strains chosen for testing of oxidant sensitivity were those with *in silico* predictions that were confirmed by experimental results (Fig. 2). Our experimental results indicate that increased basal production of O_2^- or H_2O_2 generally increases microbial susceptibility to oxidative attack (Fig. 3). Genetic deletions that increase ROS production exhibited increased susceptibility to oxidants, whereas the negative control strains that exhibited wildtype production levels of ROS did not. The probability this enrichment would have been observed by random selection is 2.5×10^{-5} (Methods), and demonstrates that increased production of O_2^- and H_2O_2 can potentiate killing by oxidants. We note that some predictions conferred increased susceptibility to all oxidants tested (*ΔcyoA* and *ΔsdhC*), whereas others exhibited selective increases in sensitivity (*e.g., Δzwf*), suggesting that sensitivity to one oxidant does not always translate to other oxidants. This is not surprising, and likely derives from the differences in biochemical activity of the oxidants and the distinct cellular death pathways they induce[20, 21]. Our results clearly demonstrate that increasing endogenous production is a robust strategy to enhance the susceptibility of microbes to oxidative stress.

Bactericidal antibiotics have been shown to share a common mechanism of cell death that involves the production of ROS[3]. We sought to determine if increased basal production of ROS could potentiate the action of bactericidal antibiotics (the β-lactam ampicillin, the fluoroquinolones ofloxacin and ciprofloxacin, and the aminoglycoside gentamicin) (Fig. 4). Three of the validated targets (*ΔcyoA, ΔnuoG, ΔsdhC*) exhibited increased sensitivity to both β-lactam and fluoroquinolone antibiotics (Fig. 4a,b and Supplementary Fig. 2a) and one of the targets (*Δpta*) exhibited increased sensitivity to only fluoroquinolones (Fig. 4b and Supplementary Fig. 2a), whereas all of the negative control strains displayed wildtype

NIH-PA Author Manuscript

NIH-PA Author Manuscript

NIH-PA Author Manuscript

sensitivity to both antibiotic classes (Fig. 4c,d and Supplementary Fig. 2b). This results in a correct prediction rate for our approach of greater than 70% for both β-lactams and fluoroquinolone antibiotics. Sensitivity to aminoglycosides was also tested, though we reasoned that increased killing, in general, would not be observed. This expectation was based on the fact that many of the gene deletions that increase basal ROS production negatively impact proton motive force, which is important for aminoglycoside uptake[22]. As expected, the negative controls had similar sensitivity to gentamicin as wildtype, whereas many targets exhibited decreased sensitivity (see Supplementary Fig. 2c,d online). We note that *ΔatpC* demonstrated increased sensitivity toward gentamicin, which we believe may be the result of its positive impact on proton motive force[23] as well as its effect on basal ROS production. These data indicate that bactericidal antibiotic primary target interactions must be enabled (*e.g.*, via antibiotic uptake) in order to leverage ROS production as an adjuvant therapy. Accordingly, we expected and demonstrated that the activities of bacteriostatic antibiotics, which do not produce ROS[6], are unaffected by increases in basal ROS production (see Supplementary Fig. 3 online).

We also sought to demonstrate that chemical inhibition of one of the validated targets could increase sensitivity to oxidants and bactericidal antibiotic treatment. To do so, we treated wildtype with carboxin, an inhibitor of succinate dehydrogenase, and measured susceptibility toward H_2O_2 and ampicillin, respectively. Addition of carboxin alone had no effect on the growth of wildtype cells (Fig. 4e, f). However, wildtype cells treated with H_2O_2 and carboxin demonstrated increased sensitivity compared to wildtype cells treated with H_2O_2 alone (Fig. 4e). Similarly, wildtype cells treated with ampicillin and carboxin were significantly more sensitive to the antibiotic than cells treated with ampicillin alone (Fig. 4f). To more fully examine this synergy, we conducted a systematic drug screen spanning five concentrations for each compound (carboxin and ampicillin) including the untreated sample. This allowed us to calculate that carboxin concentrations of 250μM or greater are synergistic with ampicillin concentrations between 7.5–10 μg/mL, using the Bliss Independence and Highest Single Agent models of drug synergism (see Supplementary Fig. 4 online). These results show that chemical inhibition of a predicted and validated target (succinate dehydrogenase) is sufficient to increase sensitivity to oxidative attack and antibiotic treatment. Although carboxin itself is not suitable as an antibiotic adjuvant owing to human toxicity issues[24], validation that chemical inhibition of succinate dehydrogenase confers similar sensitivity as genetic perturbation allows translation of this finding to chemical library screening where non-toxic inhibitors of bacterial succinate dehydrogenase and other predicted targets may be found. Chemical libraries have been successfully screened for compounds with antimicrobial properties against pathogenic bacteria[25] and our method complements this work by identifying novel enzyme targets for compounds which may have no antimicrobial properties alone, but which enhance the killing efficacy of current antibacterial agents.

Here we established a systems-based method to predictably tune microbial ROS production. By developing genome-scale ROS metabolic models, we were able to predict redistribution of ROS flux resulting from network perturbations and demonstrate experimentally that increased ROS flux can potentiate oxidative attack from antibiotic and biocide treatment. This approach allows rapid identification of antibacterial adjuvant targets, and is translatable to other pathogens of interest, such as *Mycobacterium tuberculosis, Staphylococcus aureus, Haemophilus influenzae*, and *Salmonella typhimurium*, where metabolic reconstructions are available[26–29]. In addition, the increasingly rapid construction of genome-scale metabolic models will extend the breadth of the technique[30], opening up the possibility of using it to target newly identified resistant strains.

NIH-PA Author Manuscript

NIH-PA Author Manuscript

NIH-PA Author Manuscript

Online Methods

Antibiotics and chemicals

All chemicals and antibiotics were purchased from Sigma or Fisher Scientific. Concentrated stock solutions of menadione, H_2O_2, NaOCl, and all antibiotics were prepared fresh daily. H_2O_2, NaOCl, ampicillin, and gentamicin were diluted with or dissolved in sterile deionized water. Ofloxacin and ciprofloxacin were dissolved in 0.1N NaOH. Tetracycline was dissolved in 50% ethanol (v/v). Menadione, carboxin, and chloramphenicol were dissolved in 100% ethanol.

Strains and media

Escherichia coli MG1655 was used in this study. Genetic deletions of *aceA, appB, atpC, cyoA, edd, fumB, fbaB, gdhA, gltB, gnd, mqo, nuoG, pfkB, pta, pykA, rpiB, sdhC, sucC, talB, tktB* and *zwf* were transduced from the Keio single-gene deletion knockout library[31] into MG1655 using the P1 phage method, and confirmed with PCR. The media used for all experiments was M9 minimal media with 10mM glucose as the sole carbon source or MOPS minimal media with 10mM glucose (for the HyPer protein experiments).

Plasmids

The O_2^- response sensor used in this study was constructed previously[7], and utilized the native *soxS* promoter upstream of the *gfpmut2* gene. The H_2O_2 response sensor used the same plasmid backbone and was constructed by PCR-amplifying the native *dps* promoter and cloning it into the BamHI and XhoI restriction sites, which formerly contained the *soxS* promoter. The forward primer for PCR was GCGCCTCGAGCCGCTTCAATGGGGTCTACGCT and the reverse primer was GGCCGGATCCTCGGAGACATCGTTGCGGGTAT. The H_2O_2 response sensor was confirmed to increase expression of GFP upon addition of H_2O_2.

GFP reporter assays

Fluorescent measurements were performed on a SpectraMax M5 plate reader (Molecular Devices) using Costar black, clear, flat bottom 96-well plates (Fisher). Each well contained 195μL of M9 minimal glucose media with ampicillin (100μg/mL) and 5μL of overnight culture (plasmids carry an AmpR gene for selection). Overnight cultures were grown in M9 minimal glucose media. Strains were grown in the plate reader at 37°C with shaking. OD_{600} and fluorescence (excitation: 488nm, emission: 520nm, bottom read) were monitored every 10 minutes. Fluorescence/OD_{600} values were calculated using ordinary least squares regression for measurements between OD_{600} = 0.1 and OD_{600} = 0.4. Values reported in Supplementary Table 2 are the relative mean and standard error mean for at least three independent biological replicates. P-values were calculated using a single-tailed, two-sample t-test, assuming unequal variance.

HyPer assays

The HyPer protein is a fluorescent probe that was made by inserting a circularly permuted yellow fluorescent protein into the H_2O_2-sensitive regulatory domain of OxyR[32]. In the presence of increasing concentrations of H_2O_2, the probe's excitation peak shifts ratiometrically from 420nm to 500nm, which allows for quantitative measurement of cellular H_2O_2 levels[32, 33]. HyPer is based on an *E. coli* H_2O_2-sensing domain, and has been shown to be effective at sensing H_2O_2 within *E. coli*[32]. HyPer was provided from the manufacturer (Evrogen) as an IPTG-inducible gene in a pQE30 vector (ampicillin selection marker)[32]. Single colonies of strains were inoculated into LB media supplemented with 50μg/mL ampicillin and grown overnight at 37°C. The *ΔatpC* and *Δzwf* strains were run

NIH-PA Author Manuscript

NIH-PA Author Manuscript

NIH-PA Author Manuscript

separately with wildtype because those strains grew significantly slower than the other mutant strains. Strains were inoculated 1:100 into MOPS minimal media plus 10mM Glucose and 50μg/mL ampicillin, and grown to an OD_{600} of 0.2–0.3. All cultures were then diluted with MOPS minimal media plus 50μg/mL ampicillin in a black, clear bottom 96-well plate to a final OD_{600} of 0.05, in a final volume of 200μL per well. 20μL of mineral oil (Sigma Aldrich) was added to each well to prevent evaporation. Strains were grown with and without 75μM IPTG in a SpectraMax M5 plate reader (Molecular Devices) at 37°C with shaking, and OD_{600} and fluorescence (excitation: 420nm and 500nm, emission: 530nm, bottom read) were monitored every 15 minutes for 12 hours. Measurements between OD_{600} = 0.2 and OD_{600} = 0.6 were corrected for background strain fluorescence by subtracting the fluorescence values for un-induced cultures at the same cell density, as measured by OD_{600}. The 420nm × 500nm curve was linear over this region, and therefore ordinary least squares regression was used to interpolate between time points. The 500nm excitation fluorescence value that corresponded with 55 fluorescence units from 420nm excitation was calculated and the 500/420 ratio was obtained for all strains. Values reported in Supplementary Table 3 are the relative mean and standard error mean for three independent biological replicates. P-values were calculated using a single-tailed, two-sample t-test, assuming unequal variance.

Antimicrobial sensitivity assays

Strains were grown aerobically from an initial inoculation of OD_{600} = 0.01 to OD_{600} = 0.16–0.20 in 250mL baffled flasks filled to $1/10^{th}$ the total volume and shaken at 300rpm at 37°C. For menadione, H_2O_2, and antibiotic sensitivity assays, time-zero samples were collected (200–400μL), then 1mL aliquots were transferred to 14mL test tubes, and appropriate volumes of menadione, H_2O_2, or antibiotic stock solutions, not in excess of 15μL, were added to obtain the final concentrations (1mM menadione, 5mM H_2O_2, 7.5 μg/mL ampicillin, 100 ng/mL ofloxacin, 15ng/mL ciprofloxacin, 500 ng/mL gentamicin, 10 μg/mL tetracycline, and 15 μg/mL chloramphenicol). For NaOCl, due to its reactivity with media components[34], 10mL of culture was centrifuged at 3,000 rpm for 10 minutes in a benchtop centrifuge, 9.5mL of the supernatant was removed and the cell pellet was resuspended with 9.5mL of sterile phosphate buffered saline (PBS) at pH 7.2. The suspension was spun down again at 3,000 rpm for 10 minutes, and 9.5mL of the supernatant removed. The cell pellet was resuspended with 4.5mL of sterile PBS. The cell density was adjusted with sterile PBS to achieve an OD_{600} = 0.2. Time-zero samples were collected (200–400μL), 1mL aliquots were transferred to 14mL test tubes, and NaOCl stock solution was added to obtain the final concentration (20μM NaOCl). At the specified times (1, 2 hours for menadione, H_2O_2, NaOCl; 1, 2, 3, 4 hours for antibiotics), sample aliquots were collected (200–400μL). All samples were immediately centrifuged at 10k rpm in a microcentrifuge, 95% of the supernatant was removed, and the cell pellets were resuspended in PBS. Samples were serially-diluted and plated on LB agar plates, which were then incubated overnight at 37°C. Colony forming units were counted approximately 16–18 hours after plating.

Carboxin inhibitor experiments

Strains were grown aerobically from an initial inoculation of OD_{600} = 0.01 to OD_{600} = 0.16–0.20 in 250mL baffled flasks filled to $1/10^{th}$ the total volume and shaken at 300 rpm at 37°C. Time-zero samples were collected (200–400μL), then 1mL aliquots were transferred to 14mL test tubes. Carboxin solubilized in 100% ethanol or ethanol alone was added to the tubes. Carboxin was added at a final concentration of 500 μM. H_2O_2 or ampicillin stock solutions were added to obtain the final concentrations of 5 mM H_2O_2 and 10 μg/mL ampicillin. A dose response was also performed of both carboxin (0, 250, 500, 750, and 1000 μM) and ampicillin (0, 5, 7.5, 10, and 15 μg/mL) to determine if the two compounds

NIH-PA Author Manuscript

NIH-PA Author Manuscript

NIH-PA Author Manuscript

demonstrate a synergistic interaction. Drug synergism was calculated using the Bliss Independence and Highest Single Agent models[35, 36]. Specifically, the formula,

$$BIC_{AB} = A + B - AB \quad (1)$$

was used to calculate synergism with the Bliss Independence model. A and B are the effects of the two drugs in isolation, whereas, BIC_{AB} is the combined effect of the two drugs as predicted by the Bliss Independence model. If C_{AB}, the experimentally-determined combined effect of the two drugs, is > BIC_{AB}, synergy is observed. In contrast, in the Highest Single Agent model, if C_{AB} > max(A, B) synergy is observed. Since we were monitoring cell death, the quantitative effect of each compound was defined as the fractional reduction of the population, $R = 1\text{-}CFU_t/CFU_0$, where CFU_t is the number of CFUs measured after treatment, and CFU_0 is the number of CFUs measured before treatment. R = 1 indicates complete loss of the population, R = 0 indicates a population in stasis, and R < 0 indicates a growing population. Since carboxin was non-lethal and allowed significant growth, even at concentrations as high as 1mM, the Highest Single Agent model was a much more stringent measure of synergy than the Bliss Independence model. To prove this, let us rewrite the Bliss Independence model as follows,

$$BIC_{AB} = A(1 - B) + B \quad (2)$$

If A is a compound that reduces CFUs, such as ampicillin, its effect above the MIC will be $0 \leq A \leq 1$, whereas if B is a compound that allows growth at all concentrations, its effect will be B < 0 regardless of the concentration. Rearrangement of the above yields,

$$BIC_{AB}/A = 1 - B + B/A \quad (3)$$

Since equation 3 yields $BIC_{AB}/A < 1$ for all $B<0$ and $0<A<1$, the Highest Single Agent model requires $C_{AB}/A > 1$ and the Bliss Independence model requires $C_{AB}/BIC_{AB} > 1$ for synergy, the Highest Single Agent model will always be a more strict synergy requirement under these conditions. Synergy can readily be observed from the relative survival curves in Supplementary Figure 4 (curves substantially lower than 1) where 7.5 and 10 μg/mL ampicillin synergize with carboxin concentrations from 250–1000μM.

Modeling *Escherichia coli* ROS metabolism

Systems-level metabolic modeling was performed using FBA and the COBRA Toolbox[37]. Aerobic *E. coli* metabolism (O_2 uptake = −18.5 mmol/gDW/hr[17]) was modeled using iAF1260 with glucose (glucose uptake = −11 mmol/gDW/hr[17]) and ammonia as the sole carbon and nitrogen sources. The model was augmented with ROS-generating reactions as described in the Supplementary Methods. Single-gene deletion analysis was performed using the built-in COBRA function. Complete modeling details are provided in the Supplementary Methods.

Statistical analysis of model performance

Statistical significance was assessed using the null hypothesis that random selection of genes would match experimental results as well as predictions from our modeling approach. For the GFP reporter systems, where *N* genes exhibited an increased ROS/BM compared to wildtype (p-value < 0.05), and *M* genes did not (*N+M*: total number of genes tested), we identified the number of genes, *P*, our approach predicted to increase ROS/BM. We calculated the (a) total number of ways to pick *P* genes from *N+M*, and then calculated the (b) number of ways to pick *P* genes that would yield *C* correct predictions, *C* being defined as the correctly predicted number of genes our approach identified to increase ROS/BM. The ratio of (b)/(a) is the probability that random selection would yield the same frequency

NIH-PA Author Manuscript

NIH-PA Author Manuscript

NIH-PA Author Manuscript

of correct predictions as our approach. Agreement was assessed by calculating the number of predictions that agreed with experimental results. For the O_2^--sensing GFP reporter, 17 of the 21 genes (81%) experimentally tested qualitatively agreed with predictions, whereas for the H_2O_2-sensing GFP reporter, 19 of the 21 genes (90%) experimentally tested qualitatively agreed with predictions. Identical procedures were used in the analysis of HyPer results, except that a p-value of 0.1 was used to identify genes that exhibited an increased H_2O_2/BM compared to wildtype. For antimicrobial sensitivity assays, statistical significance was assessed similarly, except that N in this case is the number of genes that exhibited a 2-fold increase in susceptibility toward any oxidant after a treatment time of 2 hours.

Supplementary Material

Refer to Web version on PubMed Central for supplementary material.

Acknowledgments

This work was supported by the NIH Director's Pioneer Award Program and the Howard Hughes Medical Institute.

References

1. Arias CA, Murray BE. Antibiotic-resistant bugs in the 21st century--a clinical super-challenge. N Engl J Med. 2009; 360:439–443. [PubMed: 19179312]
2. Foti JJ, Devadoss B, Winkler JA, Collins JJ, Walker GC. Oxidation of the guanine nucleotide pool underlies cell death by bactericidal antibiotics. Science. 2012; 336:315–319. [PubMed: 22517853]
3. Kohanski MA, Dwyer DJ, Hayete B, Lawrence CA, Collins JJ. A common mechanism of cellular death induced by bactericidal antibiotics. Cell. 2007; 130:797–810. [PubMed: 17803904]
4. Kohanski MA, Dwyer DJ, Wierzbowski J, Cottarel G, Collins JJ. Mistranslation of membrane proteins and two-component system activation trigger antibiotic-mediated cell death. Cell. 2008; 135:679–690. [PubMed: 19013277]
5. Carlioz A, Touati D. Isolation of superoxide dismutase mutants in Escherichia coli: is superoxide dismutase necessary for aerobic life? EMBO J. 1986; 5:623–630. [PubMed: 3011417]
6. Loewen PC. Isolation of catalase-deficient Escherichia coli mutants and genetic mapping of katE, a locus that affects catalase activity. J Bacteriol. 1984; 157:622–626. [PubMed: 6319370]
7. Dwyer DJ, Kohanski MA, Hayete B, Collins JJ. Gyrase inhibitors induce an oxidative damage cellular death pathway in Escherichia coli. Mol Syst Biol. 2007; 3:91. [PubMed: 17353933]
8. Hebrard M, Viala JP, Meresse S, Barras F, Aussel L. Redundant hydrogen peroxide scavengers contribute to Salmonella virulence and oxidative stress resistance. J Bacteriol. 2009; 191:4605–4614. [PubMed: 19447905]
9. Liu CI, et al. A cholesterol biosynthesis inhibitor blocks Staphylococcus aureus virulence. Science. 2008; 319:1391–1394. [PubMed: 18276850]
10. Imlay JA, Fridovich I. Assay of metabolic superoxide production in Escherichia coli. J Biol Chem. 1991; 266:6957–6965. [PubMed: 1849898]
11. Korshunov S, Imlay JA. Two sources of endogenous hydrogen peroxide in Escherichia coli. Mol Microbiol. 2010; 75:1389–1401. [PubMed: 20149100]
12. Massey V. Activation of molecular oxygen by flavins and flavoproteins. J Biol Chem. 1994; 269:22459–22462. [PubMed: 8077188]
13. Messner KR, Imlay JA. The identification of primary sites of superoxide and hydrogen peroxide formation in the aerobic respiratory chain and sulfite reductase complex of Escherichia coli. J Biol Chem. 1999; 274:10119–10128. [PubMed: 10187794]
14. Feist AM, Palsson BO. The growing scope of applications of genome-scale metabolic reconstructions using Escherichia coli. Nat Biotechnol. 2008; 26:659–667. [PubMed: 18536691]

NIH-PA Author Manuscript

NIH-PA Author Manuscript

NIH-PA Author Manuscript

15. Becker SA, Palsson BO. Context-specific metabolic networks are consistent with experiments. PLoS Comput Biol. 2008; 4:e1000082. [PubMed: 18483554]
16. Covert MW, Knight EM, Reed JL, Herrgard MJ, Palsson BO. Integrating high-throughput and computational data elucidates bacterial networks. Nature. 2004; 429:92–96. [PubMed: 15129285]
17. Feist AM, et al. A genome-scale metabolic reconstruction for Escherichia coli K-12 MG1655 that accounts for 1260 ORFs and thermodynamic information. Mol Syst Biol. 2007; 3:121. [PubMed: 17593909]
18. Messner KR, Imlay JA. Mechanism of superoxide and hydrogen peroxide formation by fumarate reductase, succinate dehydrogenase, and aspartate oxidase. J Biol Chem. 2002; 277:42563–42571. [PubMed: 12200425]
19. Edwards JS, Ibarra RU, Palsson BO. In silico predictions of Escherichia coli metabolic capabilities are consistent with experimental data. Nat Biotechnol. 2001; 19:125–130. [PubMed: 11175725]
20. Imlay JA. Pathways of oxidative damage. Annu Rev Microbiol. 2003; 57:395–418. [PubMed: 14527285]
21. Winter J, Ilbert M, Graf PC, Ozcelik D, Jakob U. Bleach activates a redox-regulated chaperone by oxidative protein unfolding. Cell. 2008; 135:691–701. [PubMed: 19013278]
22. Taber HW, Mueller JP, Miller PF, Arrow AS. Bacterial uptake of aminoglycoside antibiotics. Microbiol Rev. 1987; 51:439–457. [PubMed: 3325794]
23. Jensen PR, Michelsen O. Carbon and energy metabolism of atp mutants of Escherichia coli. J Bacteriol. 1992; 174:7635–7641. [PubMed: 1447134]
24. US EPA: R.E.D. Facts - Carboxin. EPA 738-F-04-010. 2004.
25. Boshoff HI, et al. The transcriptional responses of Mycobacterium tuberculosis to inhibitors of metabolism: novel insights into drug mechanisms of action. J Biol Chem. 2004; 279:40174–40184. [PubMed: 15247240]
26. AbuOun M, et al. Genome scale reconstruction of a Salmonella metabolic model: comparison of similarity and differences with a commensal Escherichia coli strain. J Biol Chem. 2009; 284:29480–29488. [PubMed: 19690172]
27. Becker SA, Palsson BO. Genome-scale reconstruction of the metabolic network in Staphylococcus aureus N315: an initial draft to the two-dimensional annotation. BMC Microbiol. 2005; 5:8. [PubMed: 15752426]
28. Jamshidi N, Palsson BO. Investigating the metabolic capabilities of Mycobacterium tuberculosis H37Rv using the in silico strain iNJ661 and proposing alternative drug targets. BMC Syst Biol. 2007; 1:26. [PubMed: 17555602]
29. Schilling CH, Palsson BO. Assessment of the metabolic capabilities of Haemophilus influenzae Rd through a genome-scale pathway analysis. J Theor Biol. 2000; 203:249–283. [PubMed: 10716908]
30. Henry CS, et al. High-throughput generation, optimization and analysis of genome-scale metabolic models. Nat Biotechnol. 2010; 28:977–982. [PubMed: 20802497]
31. Baba T, et al. Construction of Escherichia coli K-12 in-frame, single-gene knockout mutants: the Keio collection. Mol Syst Biol. 2006; 2 2006 0008.
32. Belousov VV, et al. Genetically encoded fluorescent indicator for intracellular hydrogen peroxide. Nat Methods. 2006; 3:281–286. [PubMed: 16554833]
33. Malinouski M, Zhou Y, Belousov VV, Hatfield DL, Gladyshev VN. Hydrogen peroxide probes directed to different cellular compartments. PLoS One. 2011; 6:e14564. [PubMed: 21283738]
34. Dukan S, Touati D. Hypochlorous acid stress in Escherichia coli: resistance, DNA damage, and comparison with hydrogen peroxide stress. J Bacteriol. 1996; 178:6145–6150. [PubMed: 8892812]
35. Yeh P, Kishony R. Networks from drug-drug surfaces. Mol Syst Biol. 2007; 3:85. [PubMed: 17332759]
36. Hegreness M, Shoresh N, Damian D, Hartl D, Kishony R. Accelerated evolution of resistance in multidrug environments. Proc Natl Acad Sci U S A. 2008; 105:13977–13981. [PubMed: 18779569]
37. Becker SA, et al. Quantitative prediction of cellular metabolism with constraint-based models: the COBRA Toolbox. Nat Protoc. 2007; 2:727–738. [PubMed: 17406635]

NIH-PA Author Manuscript
NIH-PA Author Manuscript
NIH-PA Author Manuscript

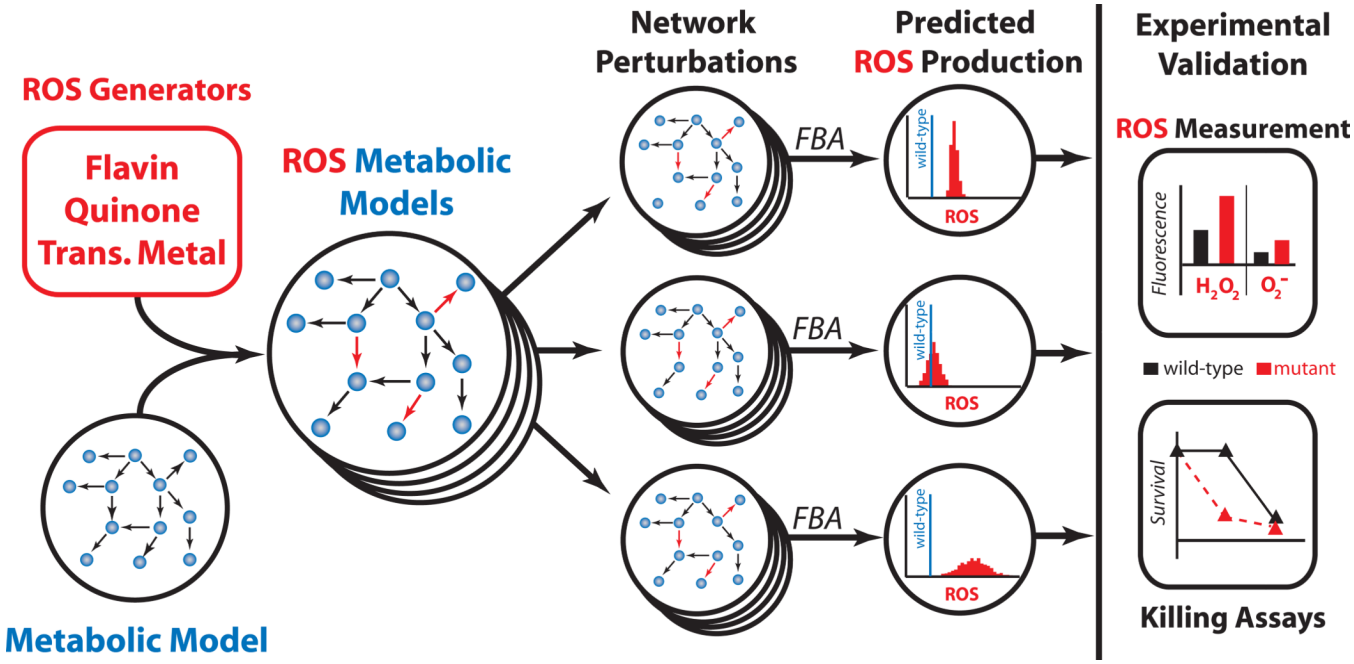

Figure 1.

Systems approach to enhance microbial ROS production. (left) Methodology for the development and validation of an ensemble of systems-level models of *E. coli* metabolism for estimation of basal ROS production. ROS-generating reactions were incorporated into a metabolic reconstruction and FBA framework[17]. Network perturbations via single-gene knockouts were performed *in silico* using FBA to identify alterations that affect ROS production. (right) *In silico* predictions were evaluated experimentally by generating mutants and measuring their ROS production and susceptibility to killing by oxidants and antibiotics.

NIH-PA Author Manuscript
NIH-PA Author Manuscript
NIH-PA Author Manuscript

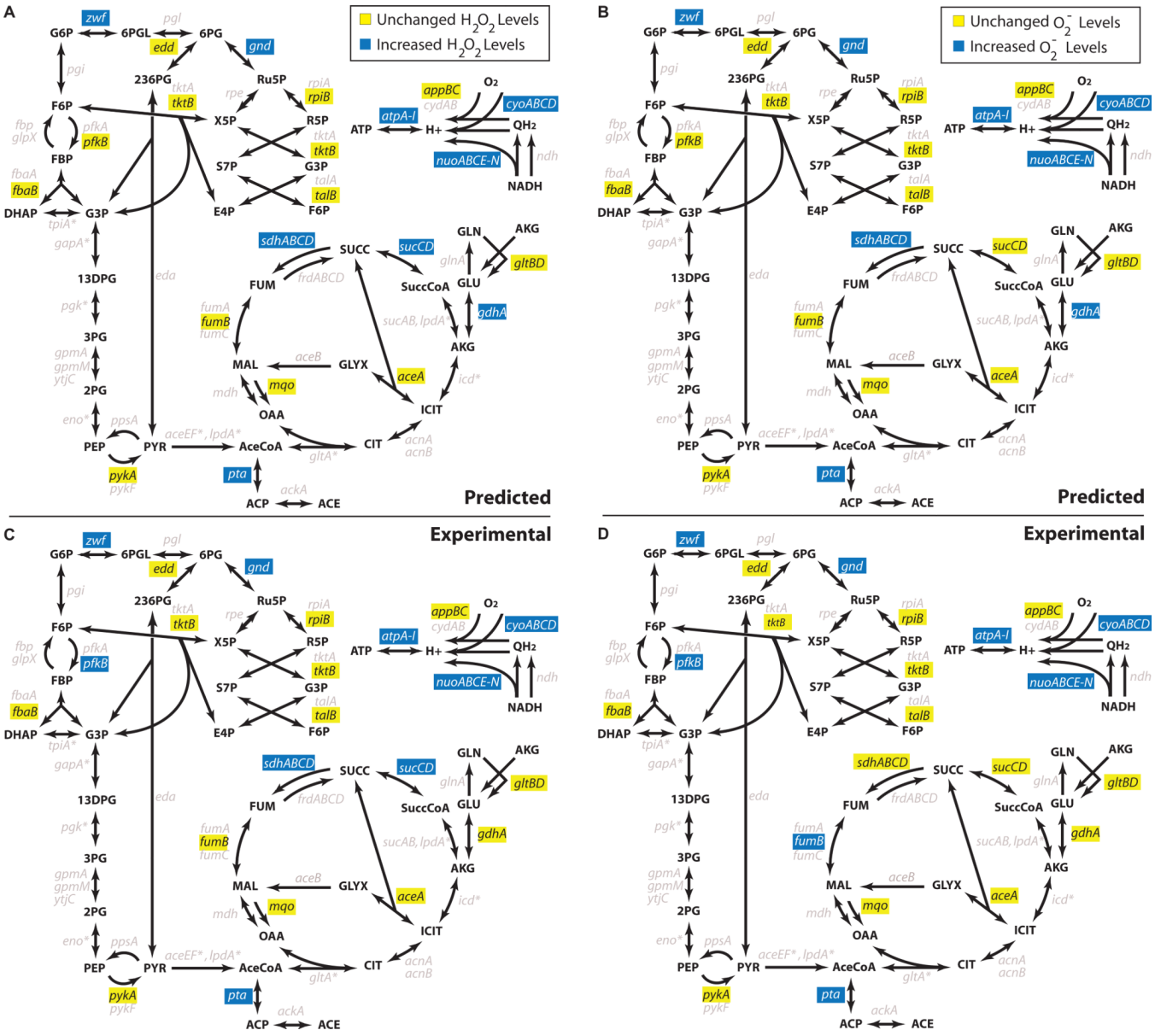

Figure 2.

In silico predictions and experimental measures of H_2O_2 and O_2^- levels. **(a)** Predicted H_2O_2 levels of various mutants compared to wildtype. Blue designates strains whose mean H_2O_2 production levels were simulated to be >5% higher than wildtype over both ensembles, whereas yellow designates strains whose mean H_2O_2 production levels were simulated to be <5% higher than wildtype over both ensembles. **(b)** Predicted O_2^- levels of various mutants compared to wildtype. Blue designates strains whose mean O_2^- production levels were simulated to be >5% higher than wildtype over both ensembles, whereas yellow designates strains whose mean O_2^- production levels were simulated to be <5% higher than wildtype over both ensembles. **(c)** Experimentally measured relative fluorescence/OD600 of strains with the H_2O_2-sensitive reporter (*dps* promoter-gfp). Blue designates strains that were experimentally measured to have increased levels of H_2O_2 compared with wildtype (P-value < 0.05), whereas yellow designates strains that were experimentally measured to have levels of H_2O_2 that do not exceed those of wildtype. **(d)** Experimentally measured relative

NIH-PA Author Manuscript

NIH-PA Author Manuscript

NIH-PA Author Manuscript

fluorescence/OD600 of strains with the O_2^--sensitive reporter (*soxS* promoter-gfp). Blue designates strains that were experimentally measured to have increased levels of O_2^- compared with wildtype (P-value < 0.05), whereas yellow designates strains that were experimentally measured to have levels of O_2^- that do not exceed those of wildtype. * denotes genes that are essential in our media conditions. Grey denotes genes that were not experimentally examined (for consistency between diagrams, these genes were also denoted by grey in **a** and **b**, although *in silico* predictions were computed).

NIH-PA Author Manuscript

NIH-PA Author Manuscript

NIH-PA Author Manuscript

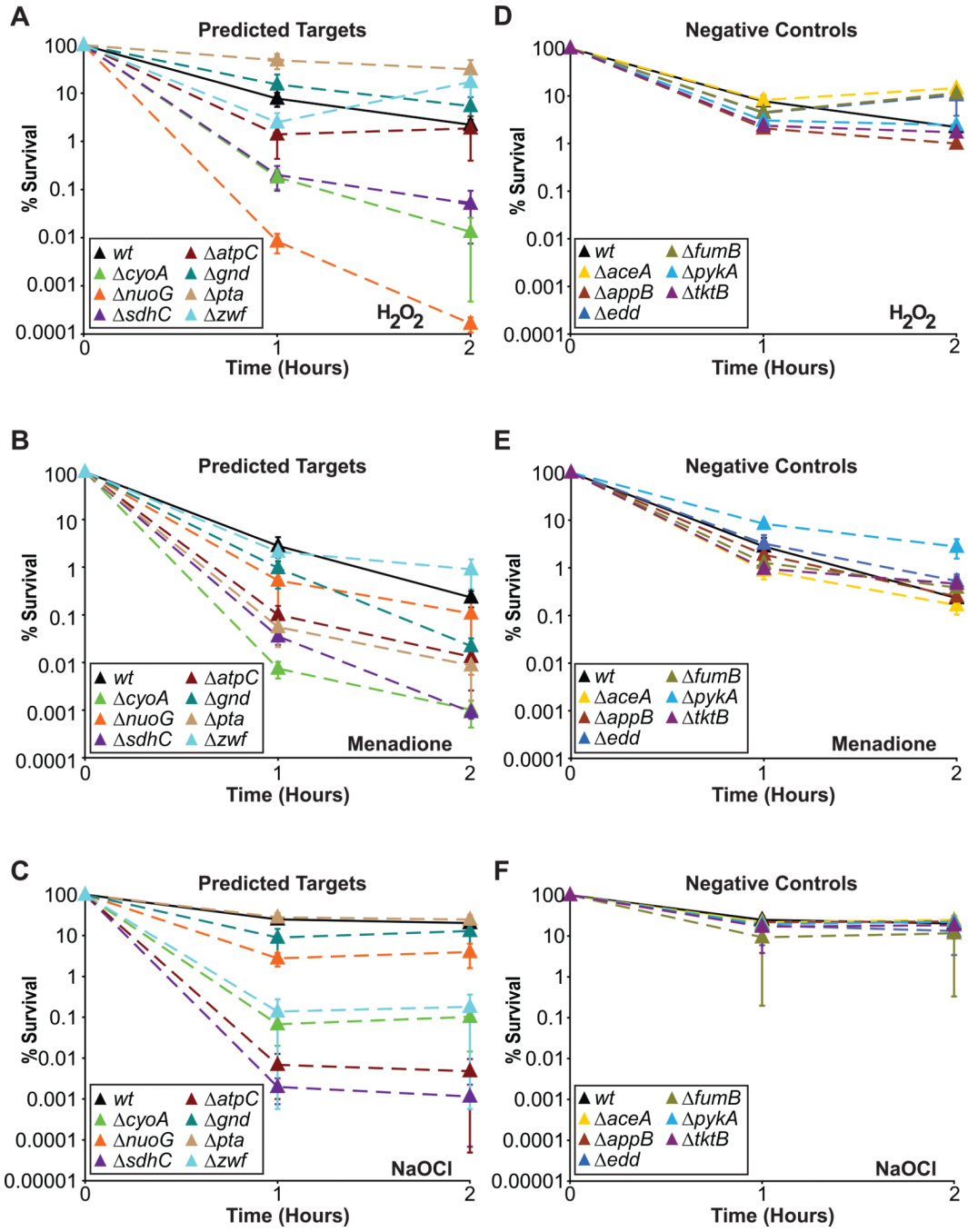

Figure 3.

Evaluation of susceptibility to killing by oxidants. **(a)** Time course of predicted target strains and wildtype treated with H_2O_2. **(b)** Time course of predicted target strains and wildtype treated with menadione. **(c)** Time course of predicted target strains and wildtype treated with NaOCl. **(d)** Time course of negative control strains and wildtype treated with H_2O_2. **(e)** Time course of negative control strains and wildtype treated with menadione. **(f)** Time course of negative control strains and wildtype treated with NaOCl. Mean ± SEM are shown for all plots.

NIH-PA Author Manuscript
NIH-PA Author Manuscript
NIH-PA Author Manuscript

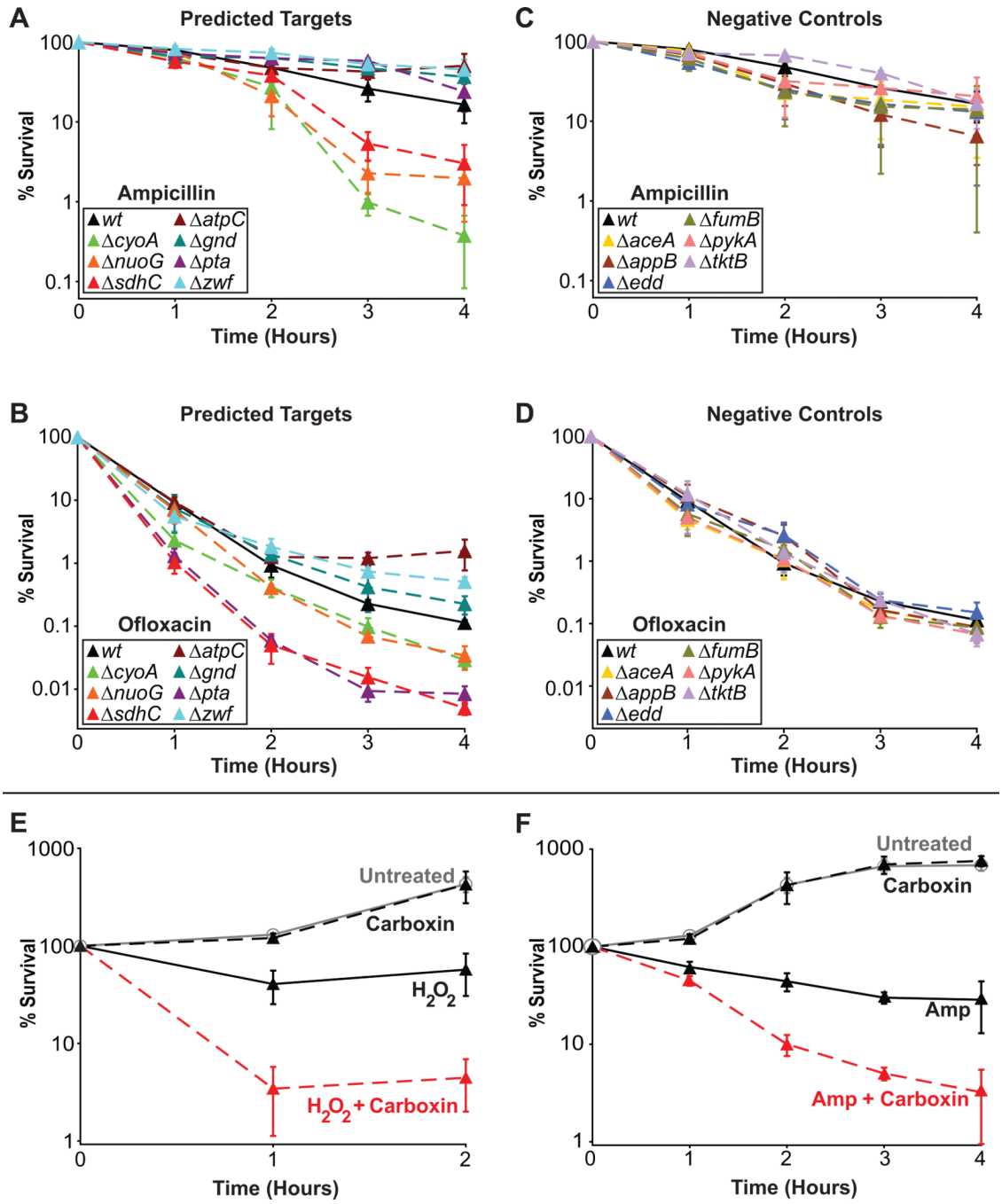

Figure 4.

Evaluation of susceptibility to killing by bactericidal antibiotics and combination treatments with a chemical inhibitor. **(a)** Time course of predicted target strains and wildtype treated with ampicillin. **(b)** Time course of predicted target strains and wildtype treated with ofloxacin. **(c)** Time course of negative control strains and wildtype treated with ampicillin. **(d)** Time course of negative control strains and wildtype treated with ofloxacin. **(e)** Time course of wildtype cells treated with carboxin alone, H_2O_2 alone, a combination of carboxin and H_2O_2, or no treatment. **(f)** Time course of wildtype cells treated with carboxin alone,

ampicillin alone, a combination of carboxin and ampicillin, or no treatment. Mean ± SEM are shown for **a–f**.

NIH-PA Author Manuscript
NIH-PA Author Manuscript
NIH-PA Author Manuscript